

## Evidence for nanoscale two-dimensional Co clusters in $\text{CoPt}_3$ films with perpendicular magnetic anisotropy

This article has been downloaded from IOPscience. Please scroll down to see the full text article.

2010 J. Phys.: Condens. Matter 22 146002

(<http://iopscience.iop.org/0953-8984/22/14/146002>)

[The Table of Contents](#) and [more related content](#) is available

Download details:

IP Address: 128.32.228.151

The article was downloaded on 23/03/2010 at 17:37

Please note that [terms and conditions apply](#).

# Evidence for nanoscale two-dimensional Co clusters in CoPt<sub>3</sub> films with perpendicular magnetic anisotropy

J O Cross<sup>1,2</sup>, M Newville<sup>3</sup>, B B Maranville<sup>4,5</sup>, C Bordel<sup>6</sup>,  
F Hellman<sup>4,6</sup> and V G Harris<sup>7</sup>

<sup>1</sup> Department of Physics, University of Washington, Seattle, WA 98195, USA

<sup>2</sup> Argonne National Laboratory, Argonne, IL 60439, USA

<sup>3</sup> Consortium for Advanced Radiation Sources, University of Chicago, Chicago, IL 60637, USA

<sup>4</sup> Department of Physics, University of California at San Diego, La Jolla, CA 92093, USA

<sup>5</sup> NIST Center for Neutron Research, Gaithersburg, MD 20899, USA

<sup>6</sup> Department of Physics, University of California at Berkeley, CA 94720, USA

<sup>7</sup> Department of Electrical and Computer Engineering, Northeastern University, Boston, MA 02115, USA

E-mail: [cbordel@berkeley.edu](mailto:cbordel@berkeley.edu)

Received 5 February 2010, in final form 19 February 2010

Published 17 March 2010

Online at [stacks.iop.org/JPhysCM/22/146002](http://stacks.iop.org/JPhysCM/22/146002)

## Abstract

The length scale of the local chemical anisotropy responsible for the growth-temperature-induced perpendicular magnetic anisotropy of face-centered cubic CoPt<sub>3</sub> alloy films was investigated using polarized extended x-ray absorption fine structure (EXAFS). These x-ray measurements were performed on a series of four (111) CoPt<sub>3</sub> films epitaxially grown on (0001) sapphire substrates. The EXAFS data show a preference for Co–Co pairs parallel to the film plane when the film exhibits magnetic anisotropy, and random chemical order otherwise. Furthermore, atomic pair correlation anisotropy was evidenced only in the EXAFS signal from the next neighbors to the absorbing Co atoms and from multiple scattering paths focused through the next neighbors. This suggests that the Co clusters are no more than a few atoms in extent in the plane and one monolayer in extent out of the plane. Our EXAFS results confirm the correlation between perpendicular magnetic anisotropy and two-dimensional Co segregation in CoPt<sub>3</sub> alloy films, and establish a length scale on the order of 10 Å for the Co clusters.

## 1. Introduction

Perpendicular magnetic anisotropy (PMA) is a pre-requisite for several possible types of magnetic storage, including magneto-optic (MO) and perpendicular recording. While it is possible to get PMA from deliberately designed materials such as multilayers and *c*-axis oriented hcp phase materials, an alternative approach is to rely on more subtle, but in many cases large, growth-induced PMA in materials such as cubic or amorphous alloys which do not *a priori* appear to support any uniaxial anisotropy.

CoPt<sub>3</sub> and similar Pt-rich Co–Pt alloys have been shown to exhibit PMA, even though CoPt<sub>3</sub> has cubic symmetry in both of its equilibrium phases—chemically disordered fcc at

high temperature and chemically ordered L1<sub>2</sub> phase below an order–disorder temperature of ~1000 K [1]. The Co–Pt system satisfies the material properties required for MO applications, including Curie temperature  $T_C$  greater than room temperature but low enough to enable diode laser writing; large Kerr rotation for robust read signals; and large coercivity to protect the written bit against accidental erasure [2–8]. In addition, Co–Pt systems, including Co/Pt multilayer structures [9, 10] and alloys [2, 3], display a pronounced magneto-optic response to blue light, a property that amorphous rare earth–transition metal alloys lack.

In the chemically disordered fcc phase of CoPt<sub>3</sub>, every Co and Pt atom is surrounded by a statistical distribution of

3 Co neighbors and 9 Pt neighbors. While this phase is in equilibrium only at high temperatures ( $>973$  K), it is easily quenched to room temperature. It has been extensively studied and shown to be ferromagnetic with a Curie temperature  $T_C$  of 483 K [11]. In the  $L_{12}$  phase, Co atoms can be considered to lie on fcc corner sites surrounded by 12 Pt neighbors at the face-center sites. This phase has also been studied and found to be ferromagnetic with  $T_C$  of 273 K when fully ordered, hence non-magnetic at room temperature due to the elimination of Co–Co nearest neighbors [1, 12]. Both of these structures are cubic and therefore do not have uniaxial magnetic anisotropy.

The PMA observed in  $\text{CoPt}_3$  alloy films is independent of the film crystallographic orientation, since it has been seen in (100), (110), and (111) epitaxial films, polycrystalline films and vicinal substrates with tilted crystallographic axes [4, 13, 14]. This growth-induced effect strongly depends on growth temperature and other deposition parameters, and vanishes upon annealing [7, 13–17]. Because the overall crystal structure in the films with PMA, as measured by both x-ray diffraction (XRD) and transmission electron microscopy (TEM), is the cubic (unstrained) fcc structure, which cannot support a uniaxial magnetic anisotropy, it is clear that local chemical anisotropy must break the apparent cubic symmetry.

All of the magnetic properties, including anisotropy, moment, and Curie temperature are extremely sensitive to the details of the local chemical ordering. Hellman *et al* showed that both the presence or absence and the magnitude of PMA correlated with an unexpected dependence of Curie temperature  $T_C$  on growth temperature  $T_g$  [4, 13]. In fact, because of the non-Brillouin-like temperature dependence of the magnetization for the samples with a high PMA, it is impossible to define  $T_C$ . The terminology of ‘magnetic onset temperature’ was therefore used to determine the temperature at which the magnetization falls to 5% of its value at 298 K [13]. The largest magnetic anisotropy constant  $K_u$  (corrected from the shape anisotropy) of  $>6 \times 10^6$  ergs  $\text{cm}^{-3}$ , which is nearly 10% of that found in the best Co/Pt multilayers, is found in  $\text{CoPt}_3$  samples for which the magnetic onset temperature is 673 K. This exceeds the magnetic onset temperature in the fcc phase by 200 K and is 400 K above that found in the chemically ordered  $L_{12}$  phase. The enormously enhanced magnetic ordering temperature suggests a substantial clustering of Co in these films, despite a known negative energy of mixing which favors the chemically mixed equilibrium state [11, 12, 18]. The high magnetic ordering temperature and the stretched decrease of the magnetization as a function of temperature are accompanied by other evidence of chemical inhomogeneity, such as substantial coercivity. The various magnetic data collected on these samples suggest a model of flat Co-rich platelets, parallel to the growth surface of the film, giving Co/Pt interfaces locally similar to a multilayer.

The underlying cause of this growth-induced effect has remained controversial for a long time [4, 5, 19, 20], but a recent work based on Monte Carlo simulations of vapor-deposited  $\text{CoPt}_3$  films supports the explanation of Co step-edge segregation, which results in Co clustering [21].

Although the model of Co nanoclusters is consistent with observed magnetization data, it has proven challenging to

observe by direct structural means. Neither TEM nor diffuse x-ray scattering, both techniques which have been successfully used to identify important features in other materials with growth-induced anisotropy effects such as hcp Co–Cr alloys, have shown any structure which could be interpreted as relevant to the anisotropy.

Tyson *et al* were the first ones to report an experimental observation of internal Co–Pt interfaces in a (111) textured  $\text{Co}_{0.28}\text{Pt}_{0.72}$  alloy film using polarized extended x-ray absorption fine structure (EXAFS) [20], but their analysis contains several inconsistencies. For example, they find that the gross structure of their sample is that of disordered  $\text{CoPt}_3$ , whereas the total number of Co–Co and Co–Pt bonds determined from their Co K EXAFS data are more consistent with the ordered  $L_{12}$  phase. Their suggested growth model in which Co forms anisotropic platelets is not supported by their EXAFS analysis results, which show an average of 0.5 Co–Co bonds parallel to the growth plane, a factor of three smaller than the average number of in-plane bonds for the disordered  $\text{CoPt}_3$  alloy.

Then Grange *et al* and Meneghini *et al* carried out experiments on two epitaxial (111)  $\text{CoPt}_3$  films grown at 690 K and 800 K, by means of angle-resolved XMCD and polarized EXAFS, respectively [7, 22]. They both reported anisotropic effects at the Co  $L_{II,III}$  and Co K edges, respectively, for the sample grown at 690 K that exhibits a high PMA. These observations support the model of anisotropic Co nanoclustering as the main source of PMA. However these studies give a very partial view of the correlation between short-range order and macroscopic magnetic properties in these alloys, because they are restricted to only one or two growth temperatures and refer to a very limited number of macroscopic data. Moreover, there was no estimate of the Co cluster size based on either experiments or numerical simulations.

In this paper, we present the results of polarized EXAFS experiments performed at the Co K and Pt  $L_{III}$  edges on four (111)  $\text{CoPt}_3$  films epitaxially grown at substrate temperatures ranging between 473 and 1073 K. This work is the continuation of a preliminary study that was carried out on  $\text{CoPt}_3$  films [23]<sup>8</sup>. Our EXAFS data are correlated to various results that were previously obtained on numerous samples grown in the same conditions [13], which gives a wide vision of the interplay between local ordering and PMA in  $\text{CoPt}_3$  thin films. One should note that although PMA was found to disappear upon annealing, we observed no significant strain deformation in any of our films, which rules out magnetoelastic anisotropy as the origin of PMA. The results of these EXAFS experiments unambiguously confirm a correlation between PMA and growth-induced two-dimensional Co segregation in  $\text{CoPt}_3$  alloy films, and establish a length scale of 6–10 Å for the size of the Co clusters. The existence of such nanoclusters supports the model of Co step-edge segregation developed by Maranville *et al* [21], arising from a three-dimensional island growth mechanism in epitaxial films [24].

<sup>8</sup> NB: the sample orientation was actually (111) instead of (100).

## 2. Experiment

The growth conditions of the epitaxial CoPt<sub>3</sub> films measured in these experiments are the same as the ones that have already been described in an earlier study [13]. Briefly, 200–300 nm thick (111) oriented films were grown by electron beam co-evaporation under ultra-high vacuum conditions on (0001) sapphire single crystal substrates at 473, 723, 873, and 1073 K. RHEED patterns observed during growth showed vertical diffraction lines with no sign of rings or low angle diffuse scattering, indicating good crystal quality for all of the films. High-resolution x-ray diffraction measurements confirmed the single crystal nature of the films, and showed an increasing mosaic spread with decreasing growth temperature. From off-axis x-ray scattering measurements, the strain was found to be less than 0.03%. Figure 4 shows  $K_u$  and  $T_C$  for the current set of samples (labeled ‘present study’) plotted for comparison with data from (100) and (111) oriented films grown on MgO and sapphire, respectively (labeled ‘previous study’) [13].

Polarized Co K and Pt L<sub>III</sub> EXAFS data were collected at the Advanced Photon Source beamline 20-ID-B [25]. The electric field  $\epsilon$  of the incoming x-ray beam was either in the film plane ( $\epsilon$  in-plane) or perpendicular to the film plane ( $\epsilon$  out-of-plane). The incident photon energy was selected using a fixed-exit Si(111) monochromator scanned simultaneously with the undulator gap. The monochromator second crystal was detuned to 35% of peak intensity to reduce third harmonic contamination. The beam size was defined by slits to  $\sim 200 \mu\text{m} \times 2 \text{mm}$  to match the footprint of the beam on the samples at  $3^\circ$  incident angle. The samples were spun at 3000 rpm to reduce Bragg diffraction contamination from the sapphire substrates. The incident intensity was measured using a 300 mm gas ionization chamber flowing He at 700 VDC. The fluorescence intensity was measured using a custom gas ionization chamber with multiple Ni mesh electrodes flowing Ar at 450 VDC and a Soller slit and filter assembly to reduce background from elastic scattering [26].

## 3. Analysis

Figures 1 and 2 show the Fourier transformed EXAFS data  $\chi(R)$  for the Co K and Pt L<sub>III</sub> edges from all four samples at both polarizations. Following standard EXAFS analysis protocol,  $\chi(k)$  were isolated from the fluorescence data using AUTOBK polynomial background removal with a McMaster correction and normalized to the absorption edge step height [27]. Fourier transforms were calculated using  $k^2$  weighting with a Hanning window function.

The local chemical anisotropy for each sample was determined quantitatively by simultaneously fitting the first-shell EXAFS from both polarizations in  $R$ -space using FEFFIT [28] with theoretical phase shifts and scattering amplitudes calculated by FEFF 7.02 [29]. An overall correction factor of  $S_0^2 = 0.75$  applied to the FEFF scattering amplitudes was determined by constraining an isotropic model to give 3 Co and 9 Pt nearest neighbors for the film grown at 1073 K, which is expected to be in the randomly ordered fcc phase.

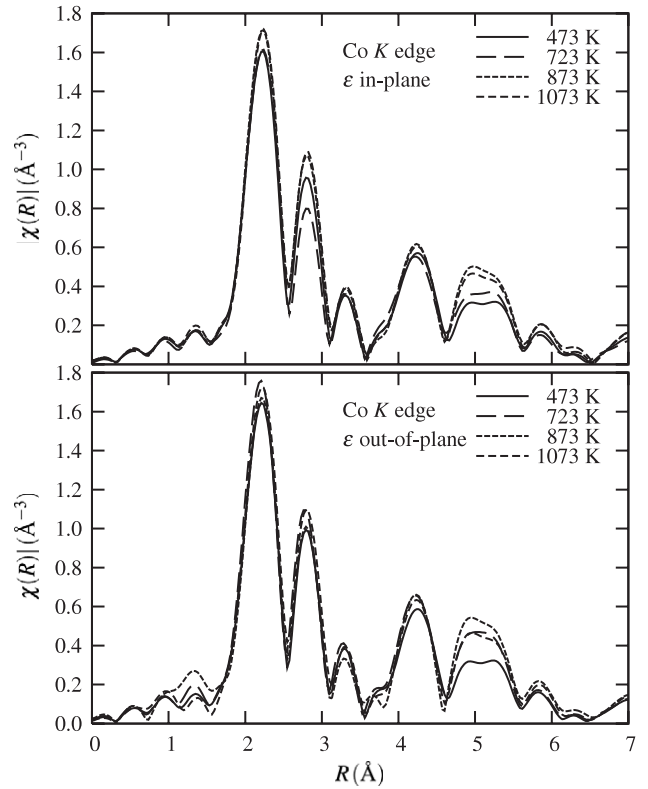


**Figure 1.** Co K-edge  $|\chi(R)|$  EXAFS data of CoPt<sub>3</sub> films. Data are shown for both in-plane (top) and out-of-plane (bottom) polarizations for films grown at 473, 723, 873, and 1073 K.  $k^2\chi(k)$  data were Fourier transformed between  $k = [1.75, 9.75] \text{ \AA}^{-1}$  with a Hanning window and  $dk = 1.25 \text{ \AA}^{-1}$ .

Fits for the Co K-edge data, shown in figure 1, were performed with an  $R$ -range of  $[1.5, 3.1] \text{ \AA}$ , a  $k$ -range of  $[1.75, 9.75] \text{ \AA}^{-1}$ , and a Hanning window width of  $1.25 \text{ \AA}^{-1}$ . The in-plane and out-of-plane polarized EXAFS were refined simultaneously for each growth temperature and absorption edge, therefore a single energy shift  $E_0$ , absorber–Co distance  $R_{\text{Co–Co}}$ , absorber–Pt distance  $R_{\text{Co–Pt}}$ , absorber–Co mean-square-displacement  $\sigma_{\text{Co–Co}}^2$ , and absorber–Pt mean-square-displacement  $\sigma_{\text{Co–Pt}}^2$  were varied for both polarizations. To account for chemical anisotropy, we defined two parameters  $\alpha$  and  $\beta$ ,  $0 \leq \alpha, \beta \leq 1$ , to represent the fraction of Co first-shell neighbors in-plane and out-of-plane, respectively. Thus we have a combined total of seven variable parameters ( $\alpha$ ,  $\beta$ ,  $E_0$ ,  $R_{\text{Co–Co}}$ ,  $R_{\text{Co–Pt}}$ ,  $\sigma_{\text{Co–Co}}^2$ , and  $\sigma_{\text{Co–Pt}}^2$ ) for each pair of polarization data sets, compared to the estimated maximum of  $\sim 10$  parameters that could be determined by a single data set based on the Fourier transform and fit range [30].

The FEFF phases and amplitudes were calculated for unpolarized incident x-rays and polarization dependence for the in-plane and out-of-plane paths was explicitly built into the Co K (equation (1)) and Pt L<sub>III</sub> (equation (2)) models. In K-shell absorption, the polarization dependence for the  $s \rightarrow p$  transition is  $\cos^2 \theta$ , where  $\theta$  is the angle between the polarization vector and the interatomic bond. In the (111) oriented film, an absorbing atom has six neighbors in-plane and six out-of-plane, three above and three below, at  $54.7^\circ$  from the

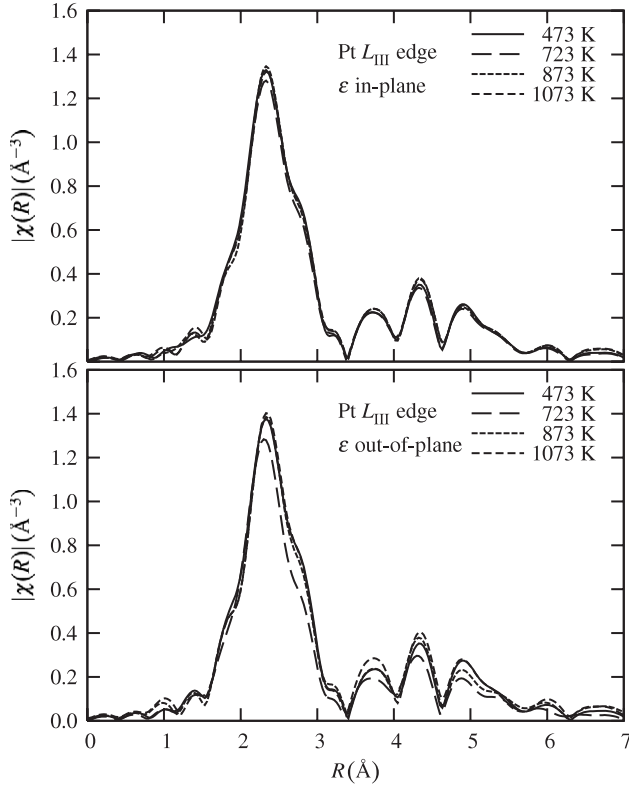


**Figure 2.** Pt  $L_{III}$ -edge  $|\chi(R)|$  EXAFS data of  $\text{CoPt}_3$  films. Data are shown for both in-plane (top) and out-of-plane (bottom) polarizations for films grown at 473, 723, 873, and 1073 K.  $k^2\chi(k)$  data were Fourier transformed between  $k = [3.0, 11.5] \text{ \AA}^{-1}$  with a Hanning window and  $dk = 1.5 \text{ \AA}^{-1}$ .

plane. The contribution to  $\chi$  of the Co–Co and Co–Pt atomic pairs for the in-plane and out-of-plane Co K-edge EXAFS for (111) oriented film in terms of  $\alpha$  and  $\beta$  can written as

$$\chi_{\parallel} = 3[(3\alpha + \beta)\chi_{\text{Co-Co}} + (4 - 3\alpha - \beta)\chi_{\text{Co-Pt}}] \quad (1a)$$

$$\chi_{\perp} = 3[4\beta\chi_{\text{Co-Co}} + 4(1 - \beta)\chi_{\text{Co-Pt}}] \quad (1b)$$

where  $\chi_{\text{Co-Co}}$  and  $\chi_{\text{Co-Pt}}$  are the unpolarized EXAFS signals calculated for a single Co–Co bond and a single Co–Pt bond embedded in the  $L_{12}$  environment.

The fit results for the in-plane and out-of-plane Co K-edge data at 723 K, which shows the largest chemical (and magnetic) anisotropy, are shown in figure 3. Note that a Ramsauer–Townsend resonance [31] in the Pt backscattering amplitude at the Co K-edge effectively splits the Pt first shell,  $R = [1.5, 3.1] \text{ \AA}$ , into two lobes, significantly improving the reliability of the fit to distinguish between Co and Pt near neighbors. The numerical results for all of the Co K-edge fits are given in table 1, and the first-shell chemical anisotropy  $\alpha - \beta$  is plotted in figure 4 along with  $K_u$  and  $T_C$  as a function of growth temperature.

The Pt  $L_{III}$ -edge data were fit using a model similar to that used for the Co K-edge. Data for in-plane and out-of-plane polarizations at each growth temperature were refined simultaneously using seven adjustable parameters ( $\alpha$ ,  $\beta$ ,  $E_0$ ,  $R_{\text{Pt-Co}}$ ,  $R_{\text{Pt-Pt}}$ ,  $\sigma_{\text{Pt-Co}}^2$ , and  $\sigma_{\text{Pt-Pt}}^2$ ). An  $R$ -range of  $[1.5, 3.1] \text{ \AA}$

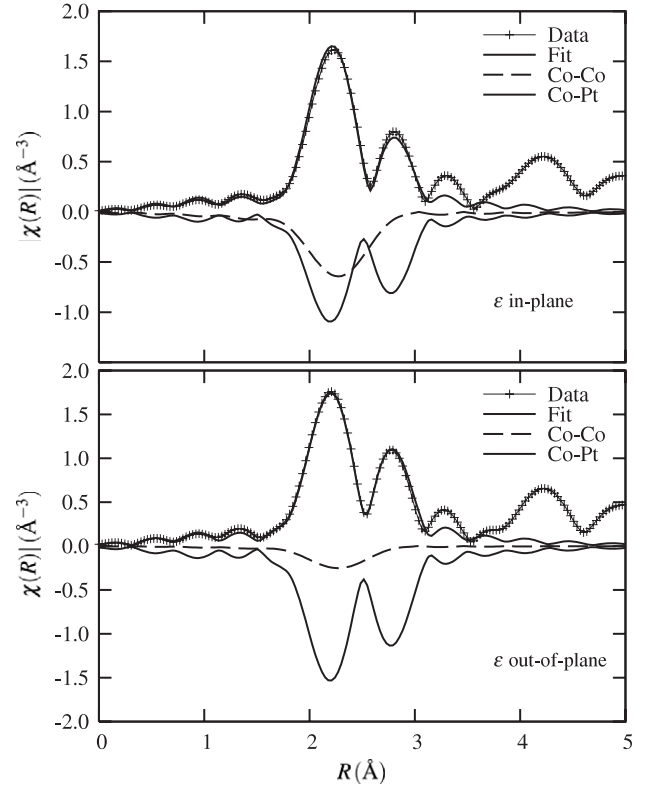


**Figure 3.** Co K-edge EXAFS  $|\chi(R)|$  data (+) and best-fit (solid) for  $\text{CoPt}_3$  film grown at 723 K. Also shown are  $-|\chi(R)|$  for the Co–Co (dashed) and Co–Pt (solid) shells. Data were taken with the x-ray polarization vector  $\epsilon$  in the film growth plane (top) and out of the growth plane (bottom). Significantly more Co–Co neighbors are seen in the growth plane than out of the growth plane.  $k^2\chi(k)$  data were Fourier transformed between  $k = [1.75, 9.75] \text{ \AA}^{-1}$  with Hanning window parameters  $dk = 1.25 \text{ \AA}^{-1}$ . The fitting model used is described in the text. The individual Co–Co and Co–Pt contributions to the first-shell EXAFS are plotted on the negative axis to emphasize the contribution of the Pt Ramsauer–Townsend resonance to the total first-shell signal.

and a  $k$ -range of  $[3.0, 11.5] \text{ \AA}^{-1}$ , with a Hanning window width of  $1.5 \text{ \AA}^{-1}$ , again suggesting that  $\sim 10$  parameters could be determined for each data set.  $S_0^2 = 0.70$  was used for the Pt  $L_{III}$ -edge, as this also gave 3 Co and 9 Pt nearest neighbors for the film grown at 1073 K.

The polarization dependence of EXAFS at  $L_{III}$  absorption edges is somewhat more complicated than for K edges, due to contributions of both  $p \rightarrow s$  and  $p \rightarrow d$  transitions, which give isotropic and  $\cos^2\theta$  contributions, respectively. The polarization dependence of the EXAFS amplitude goes as  $(\frac{1}{2} + c) + 3(\frac{1}{2} - c)\cos^2\theta$ , where  $c = |M_{10}|/|M_{12}|$  is the ratio of the amplitudes of the dipole matrix elements for  $p \rightarrow s$  and  $p \rightarrow d$  transitions [32]. For a (111) oriented fcc film, the total  $L_{III}$  EXAFS for the in-plane and out-of-plane polarized incident beam in terms of  $\alpha$  and  $\beta$  can be written as

$$\chi_{\parallel} = 3\left\{\left[\frac{1}{2}(5 - 2c)\alpha + \frac{1}{2}(3 + 2c)\beta\right]\chi_{\text{Pt-Co}} + \left[4 - \frac{1}{2}(5 - 2c)\alpha - \frac{1}{2}(3 + 2c)\beta\right]\chi_{\text{Pt-Pt}}\right\} \quad (2a)$$

$$\chi_{\perp} = 3\left\{\left[\frac{1}{2}(1 + 2c)\alpha + \frac{1}{2}(3 - 2c)\beta\right]\chi_{\text{Pt-Co}} + \left[4 - \frac{1}{2}(1 + 2c)\alpha - \frac{1}{2}(3 - 2c)\beta\right]\chi_{\text{Pt-Pt}}\right\}. \quad (2b)$$

**Table 1.** Results for fits to the first coordination shell of in-plane and out-of-plane Co K-edge data at each growth temperature. Fits were done on data for both polarizations in  $R$ -space on the range  $R = [1.5, 3.1] \text{ \AA}$ , by Fourier transforming  $k^2 \chi(k)$  data between  $k = [1.75, 9.75] \text{ \AA}^{-1}$  with Hanning window parameters  $dk = 1.25 \text{ \AA}^{-1}$ .  $S_0^2$  was fixed at 0.75 for all data. Uncertainties in all fitted parameters were estimated using standard statistical procedures, and are shown in parentheses.

$T_g$ (K)	$\alpha$	$\beta$	$E_0$ (eV)	$R_{\text{Co-Co}}$ ( $\text{\AA}$ )	$R_{\text{Co-Pt}}$ ( $\text{\AA}$ )	$\sigma_{\text{Co-Co}}^2$ ( $\text{\AA}^2$ )	$\sigma_{\text{Co-Pt}}^2$ ( $\text{\AA}^2$ )
473	0.27 (0.04)	0.24 (0.03)	1.3 (0.1)	2.66 (0.01)	2.70 (0.01)	0.018 (0.002)	0.006 (0.001)
723	0.48 (0.05)	0.16 (0.03)	1.1 (0.2)	2.67 (0.01)	2.68 (0.01)	0.014 (0.002)	0.006 (0.001)
873	0.23 (0.04)	0.28 (0.03)	1.3 (0.1)	2.66 (0.01)	2.70 (0.01)	0.019 (0.002)	0.006 (0.001)
1073	0.26 (0.05)	0.23 (0.04)	1.4 (0.2)	2.66 (0.01)	2.71 (0.01)	0.019 (0.002)	0.005 (0.001)

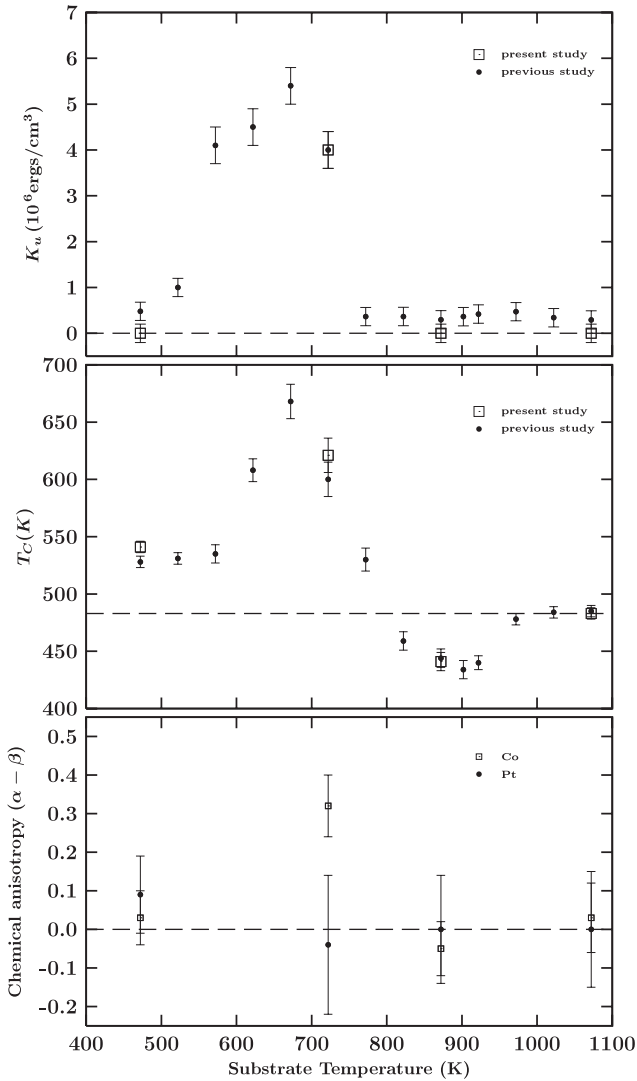


**Figure 4.** The dependence for  $\text{CoPt}_3$  films on substrate growth temperature of perpendicular magnetic anisotropy energy  $K_u$  (top), Curie temperature  $T_C$  (middle) and chemical anisotropy determined from Co K-edge and Pt  $L_{III}$ -edge EXAFS (bottom). The lines on each graph indicate the value for a homogeneous disordered alloy. The black circles displayed on the top and middle panels refer to the work previously done on similar samples [13].

This simplified formalism ignores any slight differences in phase shifts for these transitions. In the theoretical calculations from  $\text{FEFF}$ , we found little evidence for large differences in phase shifts for the Pt  $L_{III}$ -edge, which means that the frequently cited value of  $c = 0.2$  is reasonable [26].

Using equation (2) and fitting data at both polarizations together for each growth temperature, we found that the chemical anisotropy around the Pt sites is below the level of uncertainty in our fits. The results of the Pt edge fits are summarized in table 2. For all data except the 473 K data,  $\alpha$  and  $\beta$  are consistent with 0.25, corresponding to the randomly ordered fcc phase. For the 473 K data,  $\alpha$  is slightly lower than 0.25, and the number of out-of-plane Co neighbors is slightly reduced from, but still consistent with, 3. Refining separate Pt-Co and Pt-Pt distances for in-plane and out-of-plane directions gave no improvements in the fit quality and gave in-plane and out-of-plane distances that were well within the estimated uncertainty of 0.01  $\text{\AA}$ . For the 723 K data, the splitting of in-plane and out-of-plane Pt-Co distances was largest:  $\sim 0.005 \text{ \AA}$ , which is also within the estimated uncertainty, but large enough to be suggestive of a real interatomic distance anisotropy for this growth temperature. We note that Co-Pt distances seen from the Co K-edge data are slightly longer than Pt-Co distances seen from the Pt  $L_{III}$ -edge data; this small difference may reflect a small real difference in in-plane and out-of-plane Co-Pt distances, but is too small to be definitively concluded from this analysis.

The Co K-edge EXAFS data in figure 1 extend to  $R = 7 \text{ \AA}$ . As discussed above, the double peak in the region  $R = [1.5, 3.1] \text{ \AA}$  is due to photoelectron scattering from the 12 nearest neighbors of the absorbing Co atom in the fcc lattice, and the polarization anisotropy of this first-shell peak gave a quantitative measurement of the average chemical anisotropy immediately surrounding the Co atoms. The peaks at larger  $R$  are due to photoelectron scattering from more distant neighbors of the absorbing Co atom, and multiple scattering paths that include the first-shell neighbors. Quantitative structural analysis using a model similar to that used in the first shell is a problem better suited for Monte Carlo modeling, which we will not include in this paper.

Examination of figure 1 reveals significant polarization and temperature dependence in the data at 5  $\text{\AA}$ , but very little variation between samples for the peaks in the range 3.1 and 4.6  $\text{\AA}$ . The EXAFS in the range  $R = [3.1, 4.6] \text{ \AA}$  is due to scattering from atoms at the adjacent corner and opposite face of the fcc unit cell from the absorbing atom at (0, 0, 0). The peak near  $R = 5 \text{ \AA}$  is dominated by two linear multiple scattering paths from atoms at the face corners of the fcc unit cell, enhanced by forward scattering off the intermediate face-center atoms, and the intensity of the EXAFS from these so-called focusing paths is highly sensitive to the scattering strength and collinearity of the focusing atoms.

**Table 2.** Results for fits to the first coordination shell of in-plane and out-of-plane Pt L<sub>III</sub>-edge data at each growth temperature. Fits were done on data for both polarizations in  $R$ -space on the range  $R = [1.5, 3.1] \text{ \AA}$ , by Fourier transforming  $k^2 \chi(k)$  data between  $k = [3.0, 11.5] \text{ \AA}^{-1}$  with Hanning window parameters  $dk = 1.5 \text{ \AA}^{-1}$ .  $S_0^2$  was fixed at 0.70 for all data. Uncertainties in all fitted parameters were estimated using standard statistical procedures, and are shown in parentheses.

$T_g$ (K)	$\alpha$	$\beta$	$E_0$ (eV)	$R_{\text{Pt-Co}}$ ( $\text{\AA}$ )	$R_{\text{Pt-Pt}}$ ( $\text{\AA}$ )	$\sigma_{\text{Pt-Co}}^2$ ( $\text{\AA}^2$ )	$\sigma_{\text{Pt-Pt}}^2$ ( $\text{\AA}^2$ )
473	0.19 (0.05)	0.28 (0.05)	2.2 (0.3)	2.66 (0.01)	2.71 (0.01)	0.006 (0.001)	0.004 (0.001)
723	0.23 (0.09)	0.27 (0.09)	2.1 (0.6)	2.66 (0.01)	2.71 (0.01)	0.006 (0.002)	0.005 (0.001)
873	0.25 (0.07)	0.25 (0.06)	2.6 (0.4)	2.68 (0.01)	2.71 (0.01)	0.006 (0.001)	0.004 (0.001)
1073	0.25 (0.08)	0.25 (0.07)	2.4 (0.5)	2.68 (0.01)	2.71 (0.01)	0.006 (0.002)	0.004 (0.001)

Compared to the amplitude for single backscattering from first-shell neighbors, normalized to 100%, the amplitude ratios are 67% and 85% for focusing once or twice, respectively, through the intermediate first-shell atoms at the face-centered positions.

We have performed *ab initio* FEFF calculations based on the ordered L<sub>12</sub> phase, introducing first-shell chemical anisotropy based on the results from the first-shell fits. We find that the anisotropy in the higher shells is fully accounted for by the decrease in amplitude from the focusing paths where a Co atom replaces a Pt atom in the first shell. The intermediate shell, which involves scattering from third-shell atoms, both in-plane and out-of-plane, linear and triangular scattering paths, shows no anisotropy. This suggests the Co clusters are small and confined to a single atomic plane. This is consistent with the huge Co moment enhancement reported in previous studies [7, 13]. Based on the anisotropy  $\alpha - \beta$  of 0.48 for the 723 K sample determined from the EXAFS data, the average Co cluster size is four planar coordinated atoms. However, since EXAFS does not distinguish between Co in regions contributing to PMA and other Co atoms, the clusters responsible for the PMA could be slightly larger.

To summarize, the polarized EXAFS data obtained at the Co K-edge on the film grown at  $T_g = 723 \text{ K}$ , show that the spatial distribution of the Co–Co and Co–Pt bonds is not isotropic, while it is isotropic for those grown at other  $T_g$ , correlating with PMA measurements. The sample grown at  $T_g = 723 \text{ K}$  exhibits a larger number of in-plane Co–Co bonds and out-of-plane Co–Pt bonds. The signal was found to be mainly due to the first shell of nearest neighbors, and analysis shows that the Co clusters are planar with an average size on the order of 10  $\text{\AA}$ .

#### 4. Conclusion

Our EXAFS measurements unambiguously show that the growth-temperature-induced magnetic anisotropy is due to Co clustering parallel to the growth surface. The absence of chemical anisotropy in the second and third-shell EXAFS signal, which is due to scattering from out-of-plane face-centered neighbors, shows that the anisotropy is strictly two-dimensional. Furthermore, the fact that the chemical anisotropy observed in the first shell is echoed only in the fourth shell, which is dominated by multiple scattering paths focused through the first shell, implies that the two-dimensional Co clusters do not extend beyond first near

neighbors. These three observations suggest compact planar clusters averaging around four Co atoms as the most likely configuration responsible for the observed magnetic behavior.

#### Acknowledgments

We would like to thank the Director, Office of Science, Office of Basic Energy Sciences, Materials Sciences and Engineering Division, of US Department of Energy for supporting: (i) the use of PNC-CAT and the Advanced Photon Source under Contract No. W-31-109-Eng-38 and Contract No. DE-AC02-06CH11357; (ii) BBM and FH for the sample preparation and magnetic characterizations under Contract No. DE-FG02-04ER46100; (iii) CB and FH for characterization and analysis under Contract No. DE-AC02-05CH11231. The PNC-CAT beamlines are also supported by funding from the National Science Foundation, the University of Washington, the Natural Sciences and Engineering Research Council in Canada, and Simon Fraser University. The authors also acknowledge and thank J W Freeland, Y U Idzerda, S Stadler, S Sinha and J Kortright for critical discussions about x-ray diffuse scattering on these samples; E T Yu and D M Schaadt for AFM images and valuable discussion of their interpretation; and B Culbertson for RBS measurements.

#### References

- [1] Hansen M and Anderko K 1958 *Constitution of Binary Alloys* (New York: McGraw-Hill)
- [2] Lin C J and Gorman G L 1992 *Appl. Phys. Lett.* **61** 1600
- [3] Weller D, Brandle H, Gorman G, Lin C J and Notarys H 1992 *Appl. Phys. Lett.* **61** 2726–8
- [4] Rooney P W, Shapiro A L, Tran M Q and Hellman F 1995 *Phys. Rev. Lett.* **75** 1843
- [5] Maret M, Cadeville M C, Poinso R, Herr A, Beaurepaire E and Monier C 1997 *J. Magn. Magn. Mater.* **166** 45
- [6] Meneghini C, Maret M, Cadeville M C and Hazemann J L 1997 *J. Phys. Coll. IV* **7** C2 1115
- [7] Grange W, Maret M, Kappler J-P, Vogel J, Fontaine A, Petroff F, Krill G, Rogalev A, Goulon J, Finazzi M and Brookes N B 1997 *Phys. Rev. B* **58** 6298
- [8] Ming L, Zhihong J, Zhiqiang Z and Defang S 1997 *J. Magn. Magn. Mater.* **176** 331
- [9] Carcia P F 1988 *J. Appl. Phys.* **63** 5066
- [10] Zeper W B, van Kesteren H W, Jacobs B A, Spruit J H M and Carcia P F 1991 *J. Appl. Phys.* **70** 2264

- [11] Sanchez J M, Moran-Lopez J L, Leroux C and Cadeville M C 1989 *J. Phys.: Condens. Matter* **1** 491
- [12] Berg H and Cohen J B 1972 *Metall. Trans.* **3** 1797
- [13] Shapiro A L, Rooney P W, Tran M Q, Hellman F, Ring K M, Kavanaugh K L, Rellinghaus B and Weller D 1999 *Phys. Rev. B* **60** 12826
- [14] Maranville B B, Shapiro A L, Hellman F, Schaadt D M and Yu E T 2002 *Appl. Phys. Lett.* **81** 517
- [15] Maranville B B and Hellman F 2002 *Appl. Phys. Lett.* **81** 4011
- [16] Vasumathi D, Maranville B B and Hellman F 2001 *Appl. Phys. Lett.* **79** 2782
- [17] Vasumathi D, Shapiro A L, Maranville B B and Hellman F 2001 *J. Magn. Magn. Mater.* **223** 221
- [18] Cadeville M C and Moran-Lopez J L 1987 *Phys. Rep.* **153** 331
- [19] DeSantis M, Baudoing-Savois R, Dolle P and Saint-Lager M C 2002 *Phys. Rev. B* **66** 854121
- [20] Tyson T A, Conradson S D, Farrow R F C and Jones B A 1996 *Phys. Rev. B* **54** R3702
- [21] Maranville B B, Schuerman M and Hellman F 2006 *Phys. Rev. B* **73** 104435
- [22] Meneghini C, Maret M, Parasote V, Cadeville M C, Hazemann J L, Cortes R and Colonna S 1999 *Eur. Phys. J. B* **7** 347
- [23] Cross J O, Newville M, Hellman F, Rooney P W, Shapiro A L and Harris V G 2001 *J. Synchrotron Radiat.* **8** 880–2
- [24] Maranville B B 2003 *PhD Thesis* University of California at San Diego
- [25] Heald S M, Stern E A, Brewster D, Gordon R A, Crozier E D, Jiang D and Cross J O 2001 *J. Synchrotron Radiat.* **8** 342
- [26] Heald S M and Stern E A 1977 *Phys. Rev. B* **16** 5549
- [27] Newville M, Livins P, Yacoby Y, Stern E A and Rehr J J 1993 *Phys. Rev. B* **47** 14126
- [28] Newville M, Ravel B, Haskel D, Rehr J J, Stern E A and Yacoby Y 1995 *Physica B* **208/209** 154
- [29] Ankudinov A L and Rehr J J 1997 *Phys. Rev. B* **56** R1712
- [30] Stern E A 1993 *Phys. Rev. B* **48** 9825–7
- [31] McKale A G, Veal B W, Paulikas A P and Chan S K 1988 *Phys. Rev. B* **38** 10919
- [32] Stern E A and Heald S M 1983 Basic principles and applications of EXAFS *Handbook of Synchrotron Radiation* ed E E Koch (New York: North-Holland) p 995